ACS APPLIED MATERIALS & INTERFACES

www.acsami.org

Research Article

Porosity of Solid Electrolyte Interphases on Alkali Metal Electrodes with Liquid Electrolytes

Kyungmi Lim, Bernhard Fenk, Jelena Popovic,* and Joachim Maier

Cite This: *ACS Appl. Mater. Interfaces* 2021, 13, 51767−51774

Read Online

ACCESS | Metrics & More | Article Recommendations | Supporting Information

ABSTRACT: Despite the fact that solid electrolyte interphases (SEIs) on alkali metals (Li and Na) are of great importance in the utilization of batteries with high energy density, growth mechanism of SEIs under an open-circuit potential important for the shelf life and the nature of ionic transport through SEIs are yet poorly understood. In this work, SEIs on Li/Na formed by bringing the electrodes in contact with ether- and carbonate-based electrolyte in symmetric cells were systematically investigated using diverse electrochemical/chemical characterization techniques. Electrochemical impedance spectroscopy (EIS) measurements linked with activation energy determination and cross-section images of Li/Na electrodes measured by ex situ FIB-SEM revealed the liquid/solid composite nature of SEIs, indicating their porosity. SEIs on Na electrodes are shown to be more porous compared to the ones on Li in both carbonate and glyme-based electrolytes. Nonpassivating nature of such SEIs is detrimental for the performance of alkali metal batteries. We laid special emphasis on evaluating time-dependent activation energy using EIS.

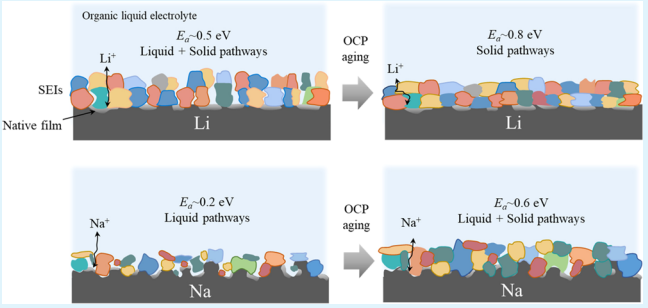

KEYWORDS: *solid electrolyte interphase, alkali metal electrodes, liquid electrolytes, battery interfaces*

1. INTRODUCTION

Alkali metals find renewed intention as most promising anode materials in battery technology. Among them, Li and Na have exceptionally high theoretical gravimetric capacities (3860 and 1166 mAh g^{-1}, respectively) and low redox potentials (−3.04 and − 2.71 V vs the standard hydrogen electrode, respectively), which makes them attractive material options for achieving high-energy-density batteries.[1,2] However, their electron configuration leads to chemical reactions with the atmosphere in which they are stored and with most electrolytes, resulting in the formation of passivating films on their surface called solid electrolyte interphases (SEIs) in the battery material research community. The physicochemical properties of the SEI play a crucial role in the performance of metal battery cells. Since SEI formation is responsible for the initial capacity loss and poor ionic transport through the SEI causes substantial additional resistance, the general aim is to form a highly ionically conductive as well as electrochemically and morphologically stable SEI.[3] Therefore, fundamental insights into the mechanism of formation and ion transport in the SEI are crucial for potential utilization of Li and Na metal batteries.[4]

Ever since Peled had first proposed a multicomponent SEI model on anodes upon contact with nonaqueous electrolytes in 1979,[5] a number of attempts have been made to understand the structure and properties of SEIs using various tools including electrochemical methods,[6−10] surface-sensitive methods such as X-ray photoelectron spectroscopy (XPS)[11,12] and infrared spectroscopy,[13] and various types of electron microscopies.[14] Based on these experimental investigations, multilayer[7] and mosaic models[15] were suggested already in the early stages of SEI discovery. The multilayer model assumes that the SEI consists of several compact/porous layers, allowing for electrochemical impedance spectroscopy (EIS) measurements to be fitted into a series of parallel RC circuits, while the mosaic model suggests a more complex distribution of the organic/inorganic SEI components. Diverse and more advanced experimental/theoretical (e.g., in situ/in operando X-ray characterization techniques, cryo-electron microscopy, atomic force microscopy, liquid secondary ion mass spectroscopy, and ab initio molecular dynamics simulations) tools have recently been introduced, allowing researchers to take a step closer in understanding the nature of SEIs on Li and Na.[16−22] However, there is still a lack of fundamental understanding of the growth mechanism of SEIs on Li/Na metals, especially under open-circuit potential.[23,24] The ability to maintain the capacity of batteries under this condition, the so-called shelf

Received: August 16, 2021
Accepted: October 6, 2021
Published: October 20, 2021

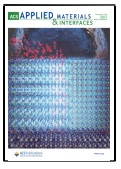

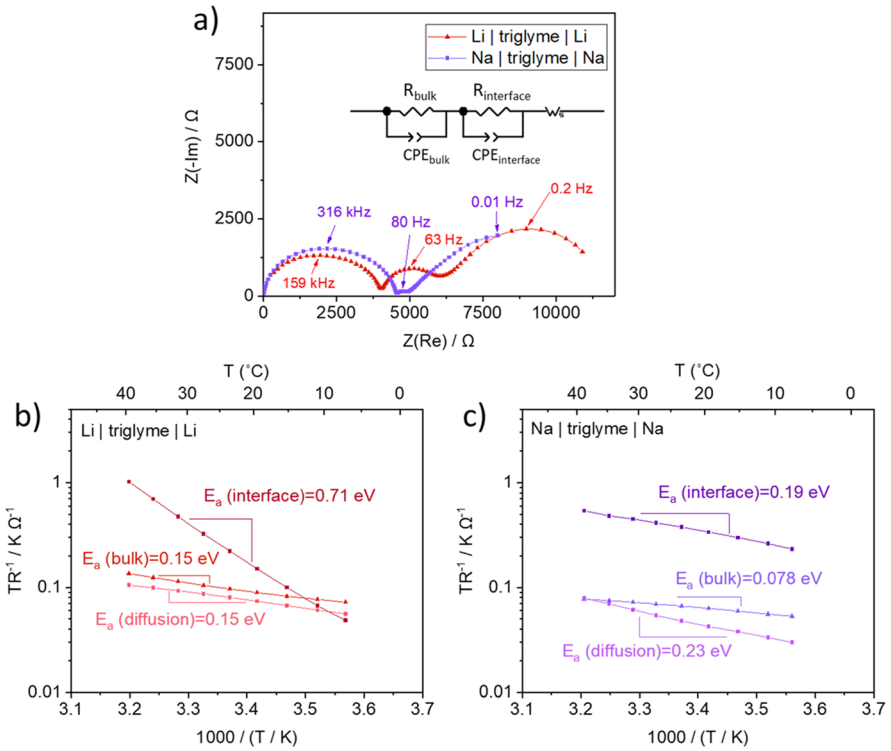

Figure 1. Investigation of symmetric Li/Na cells containing pure triglyme with EIS. (a) Nyquist plots with the characteristic frequency responses. The inset shows the corresponding equivalent circuit (R: resistance, CPE: constant phase element, W_s: finite-length Warburg response with short circuit terminus). (b,c) Arrhenius plots and E_a of different contributions observed in (a) corresponding to bulk, interface, and Li(Na) diffusion. The cells were measured after 150 h of storage under open-circuit conditions.

life, is a crucial property needed for the utilization of Li/Na metal batteries but is often overlooked. Furthermore, systematic study of the growth/transport mechanism of SEIs on Li vs Na has yet to be done. Recently, the SEI on Na formed by liquid electrolyte has been shown to be less chemically/mechanically stable compared to the SEI on Li[25,26] and has even been reported to dissolve into specific liquid electrolytes.[25,27] However, most of the abovementioned claims are based on indirect evidence, without thorough analysis involving combination of electrochemical/chemical/morphological characterization.

In this work, we investigate the growth and transport mechanism of the SEI on Li and Na in contact with glyme- and carbonate-based electrolytes. The first electrolyte class is typically used in metal−sulfur and metal−oxygen cells, while the latter is a common class of electrolytes known in lithium-ion batteries since their commercialization in 1990s. EIS with small amplitudes (10 mV) is applied to investigate the growth mechanism under the conditions close to open-circuit potential. By combining various ex situ characterization techniques such as focused ion beam-scanning electron spectroscopy (FIB-SEM), XPS, and time-of-flight secondary ion mass spectroscopy (ToF-SIMS), the SEI growth behavior is inspected in more detail. The analysis of the activation energy is shown to be the key to obtaining mechanistic insights, although rarely done in battery research. Additionally, electrolyte properties such as the cation transference number and salt diffusion coefficient (D_{salt}) were derived from the galvanostatic polarization method and low-frequency EIS, when possible.[28]

2. EXPERIMENTAL SECTION

2.1. Electrolyte and Electrode Preparation. Triethylene glycol dimethyl ether (triglyme, 99%) and molecular sieves (pore size of 3 Å, diameter of 1−2 mm) were purchased from Alfa Aesar. Ethylene carbonate (EC, 98%) and dimethyl carbonate (DMC, 98%) were purchased from Sigma-Aldrich. In order to remove the residual moisture, molecular sieves were first activated by heating to 180 °C under vacuum overnight and then added to the solvents. LiTf ($LiCF_3SO_3$, 98%, Sigma-Aldrich) and NaTf ($NaCF_3SO_3$, 99.5%, Solvionic) salts were dried prior to use (at 120 °C under vacuum, overnight). The moisture in the electrolytes was controlled to be under 20 ppm, as confirmed by Karl Fischer titration performed in an Ar-filled glovebox (atmosphere: O_2 < 0.1 ppm, H_2O < 0.1 ppm).

Due to the high reactivity of lithium and sodium metals, surface degradation is expected even in an Ar-filled glovebox. Thus, alkali metals used (Li rod with 99.9% trace metal basis and Na cubes containing mineral oil with 99.9% trace metals basis, both purchased from Sigma-Aldrich) were cut freshly each time right before the electrodes were prepared. Li and Na were subsequently sandwiched between two Celgard separators, roll-pressed to approximately the same thickness (0.15 mm), and then cut into disks with a diameter of 10 mm.

2.2. Cell Assembly. For electrochemical tests, CR2032-type coin cells made of stainless steel were assembled. Symmetric Li(Na) electrodes were attached to the stainless-steel disks with a diameter of 18 mm and were separated by a 20 μm thick Celgard separator (H2013). A constant amount of electrolyte (20 μL) was added to each cell.

2.3. Electrochemical Measurements. EIS was performed in the frequency range from 10^6 to 0.01∼1 Hz, depending on the specific cells. The experiments were conducted in the potentiostatic mode, with an amplitude of 10 mV, using Solartron 1260 and Novocontrol Alpha-A devices. Temperature-dependent EIS measurements (in the range between 5 and 50 °C) were performed using an external thermostat (Lauda RC6CP). In this setup, two thermocouples were

https://doi.org/10.1021/acsami.1c15607
ACS Appl. Mater. Interfaces 2021, 13, 51767−51774

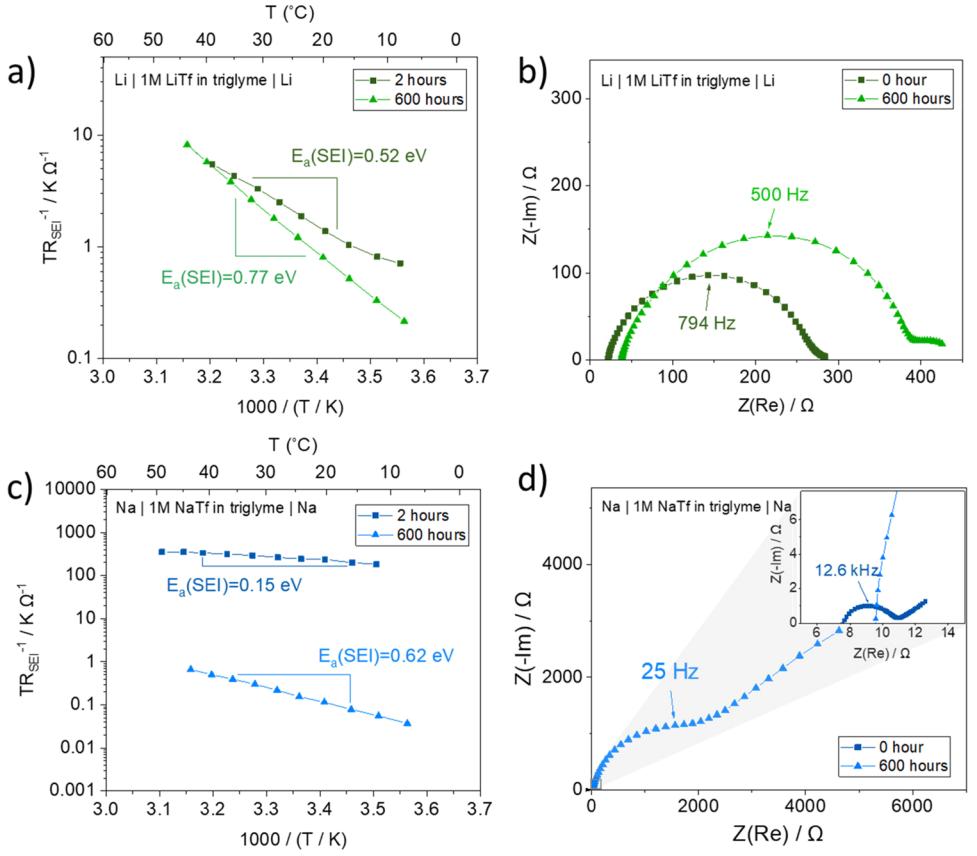

Figure 2. Evaluation of the changes in the activation energy of ion transport through SEIs. (a,c) Arrhenius plot of the Li(Na)-glyme system (symmetric Li or Na electrodes with 1 M LiTf or NaTf in triglyme) stored under open-circuit potential for 2 and 600 h. (b,d) Nyquist plots at room temperature before storage (0 h) and after storage (600 h) in the Li-glyme system and Na-glyme system, respectively.

employed: one was placed in the vicinity of the coin cell for the precise sample temperature measurement and the other was located inside a water/oil bath for control purposes. Temperature-dependent EIS measurements were carried out for 30 min for each temperature (25 min to reach the equilibrium and 5 min for EIS measurement) to minimize the changes of the SEI during the experiment. Analysis of the impedance spectra was performed with ZView software (Scribner Associates, version 3.5c).

Galvanostatic polarization was performed using a Keithley Current Source (Model 220). Galvanostatic stripping–plating tests were performed in Li/electrolyte/Li and Li/electrolyte/Cu cells by a Neware Battery Testing System (BTS V.5.3 by Neware Technology Limited) with a constant current of 0.1 mA cm^{-2}. Other parameters affecting the stripping–plating behavior such as the thickness of the electrode, the amount of liquid electrolyte, and the thickness of the separator were kept constant in every cell.

2.4. Morphological and Chemical Characterization of Surface Films. For FIB-SEM analyses, electrochemical coin cells were opened and electrodes were collected. Electrodes from the cells containing 1 M LiTf (NaTf) in triglyme and 1 M LiTf (NaTf) in EC/DMC = 50/50 (v/v) were washed with triglyme and EC/DMC = 50/50 (v/v), respectively, to avoid salt precipitation. Subsequently, they were dried under vacuum at room temperature overnight and transferred from an Ar-filled glovebox to a measurement chamber with self-made air-tight transfer tools. Cross-section images of the SEI on Li and Na metal electrodes were measured by a Zeiss Crossbeam scanning electron microscope with a built-in focused ion beam (FIB). FIB cutting was performed using a gallium beam (acceleration voltage: 30 kV) with current ranging from 200 pA to 2 nA, depending on the sample and its reactivity.

3. RESULTS AND DISCUSSION

3.1. Impedances and Activation Energies: Li/Na Electrodes in Contact with the Salt-Free Solvent. The surface of Li/Na electrodes is expected to be covered by thin (several nanometers) layers of their native oxides, hydroxides, and carbonates.[29] Even though thin layers might affect the electrolyte decomposition by differences in electron transfer,[30] their Pilling–Bedworth ratios (the ratio of molar volume of the Li/Na SEI compounds to the molar volume of the metallic Li/Na, see Supporting Information, part XII, Table S2) suggest only partial coverage. As soon as the alkali metal comes in contact with liquid electrolyte, the SEI is formed on its surface, which is not only determined by the nature of the electrode but also by the composition of the liquid electrolyte.[31,32] Typically, salt anions react with Li/Na to form inorganic compounds (e.g., MF, M_2O, M_2S, where M = Li and Na) on the surface of the electrode, while the solvent molecules tend to form organic SEI components such as polyolefins, semicarbonates, or even polymers.[31]

First, symmetric Li/Na cells containing only triglyme solvent were tested for deconvolution of the contributions from the salt and those from the solvents. Nyquist plots in Figure 1a show three distinctive features contributing to the ionic transport. The semicircle that appears at the highest frequencies (hundreds of kilohertz) corresponds to the ionic transport in the electrolyte's bulk (R_{bulk}), since its capacitance is of the order of 10^{-10} F. The decrease of R_{bulk} with time (Supporting Information, Figure S1) was observed under open-circuit conditions, most probably a consequence of the

https://doi.org/10.1021/acsami.1c15607
ACS Appl. Mater. Interfaces 2021, 13, 51767–51774

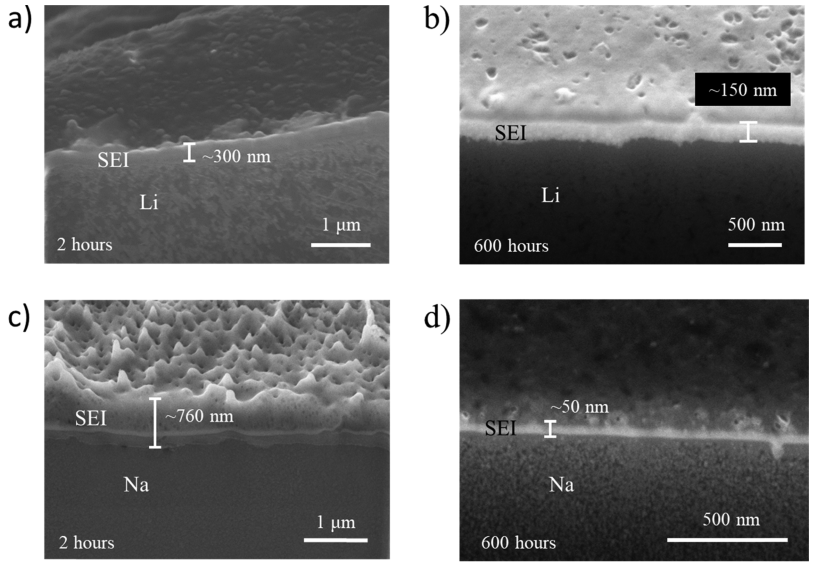

Figure 3. Cross-section images of SEIs on Li (a,b) and Na (c,d) observed by FIB-SEM. SEIs are formed by the contact between Li/Na and glyme-based electrolyte (1 M LiTf/NaTf in triglyme) and stored for 2 and 600 h.

distance decrease between two electrodes in a coin cell over time as confirmed by the experiment using a symmetric stainless-steel cell (ca. 60%, see Figure S2). Additionally, the R_{bulk} decrease could have been partially influenced by the dissolution of Li/Na from the electrode or SEI compounds, suggested by a small Li/Na concentration increase measured by inductively coupled plasma optical emission spectroscopy (ICP-OES) (see Table S1). The semicircle at medium frequency (tens of hertz) represents the ionic transport through the interfacial region, $R_{interface}$ (equivalent to the R_{SEI} used later in the text), with the capacitance in the range of 10^{-6} F.[33] As expected, $R_{interface}$ changes over time (Figure S1) due to the continuous reaction between triglyme and Li/Na. The last semicircle at low frequency (lower than 1 Hz) shows a clear Warburg-type behavior, indicating concentration polarization of salt ions within the bulk liquid in the separator. Even though such polarization effects occur in the channels of the SEI (at low frequency), they are not expected to complicate the impedance arcs of relevance for our discussion.

The clear distinction of the three contributions enabled us to measure their activation energies (E_a) by varying the cell temperature during the impedance measurement, giving further insight into their origin. Note that E_a was measured by lowering the temperature quickly (30 min for each data point) to exclude the effects of morphological or chemical changes of the SEI over time. For a symmetric Li-triglyme cell, identical E_a values were measured for the transport through bulk and polarization (0.15 eV), while the E_a of the interfacial contribution is found to be considerably higher (0.71 eV). The E_a value linked with the $R_{interface}$ formed on Na is much lower (0.19 eV) and in between the values for bulk (0.08 eV) and cationic diffusion (0.23 eV). Generally speaking, the E_a values below 0.2 eV are a clear indication of liquid ion pathways without a significant series resistance, since E_a (bulk) of the electrolytes studied here is 0.15∼0.16 eV (see Figure S4).[34,35] In summary, the results show that a more porous interface was formed in case of a Na-triglyme cell compared to a Li-triglyme cell, enabling ionic conduction through the liquid electrolyte permeated within the pores. The same measurements were performed for the case of salt-free Li-carbonate and Na-carbonate cells (see Figure S3), but a clear distinction between R_{bulk}, $R_{interface}$, and Warburg contribution was not possible due to the high total resistance amounting to MΩ.

3.2. SEI Growth and Transport in Li/Na Electrodes upon Contact with the Salt-in-Solvent Electrolyte. For a better understanding of the ionic transport properties of SEIs, salt was added to the solvent and cells of Li-glyme (Li|1 M LiTf in triglyme|Li) and Na-glyme (Na|1 M NaTf in triglyme|Na) systems were assembled and aged upon open-circuit potential, followed by measurements of activation energies and SEI thicknesses. Figure 2a shows the evolution of the E_a(SEI) over time in the case of the Li-glyme system, increasing from 0.52 to 0.77 eV after 600 h. Considering that inorganic Li SEI compounds show activation energies of ionic transport higher than 0.8 eV,[36−38] an E_a(SEI) value of 0.52 eV implies that the formed SEI is partially porous with ion transport pathways of solid and liquid phase mixtures. These values are in line with previous studies on $LiClO_4$ and $LiAsF_6$-containing electrolytes in contact with Li.[6] An increased E_a(SEI) of 0.77 eV could indicate the change of materials consisting SEIs. However, XPS surface analysis for SEIs on Li stored for 2 and 600 h under open-circuit conditions showed negligible change in the chemical composition of the SEI over time, and details can be found in the Supporting Information (Figures S8-1 and S8-2). Therefore, the increased value of E_a(SEI) is most probably the result of densification, in other words, increase of the volume fraction of SEI's solid phase. In the case of the Na-glyme system shown in Figure 2c, an exceptionally low E_a(SEI) (0.15 eV) is observed at the very initial stage of storage, which is identical to the measured E_a of ion diffusion in the bulk liquid (Figure S4). Along with a strikingly small value of E_a(SEI), an SEI resistance of 3 Ω (Figure 2d, inset) indicates that the SEI in this system is highly porous at the early stages of its growth, similarly as in the case of Na-triglyme without salt (Figure 1c). Such porous SEI allows liquid electrolyte to penetrate through it, resulting in low resistance of a liquid/solid composite at the beginning of the SEI growth. However, the liquid electrolyte continuously reacts with Na on the exposed surfaces, finally resulting in a denser and more

https://doi.org/10.1021/acsami.1c15607
ACS Appl. Mater. Interfaces 2021, 13, 51767−51774

resistive SEI as proven by higher E_a(SEI) (0.62 eV) (Figure 2c) and higher R_{SEI} (>2000 Ω) (Figure 2d).

Figure 3 shows cross-section images of SEIs on Li and Na formed by the contact with glyme-based electrolytes. A decrease in SEI thickness (300 nm to 150 nm) is evident in the Li-glyme system, indicating decreased ionic conductivity of the SEI at the end of aging, given by the increased SEI resistance (Figure 2b). On the contrary, initial porosity in the Na-glyme system is observed (Figure 3c), followed by a thinner and more compact SEI after 600 h of storage (Figure 3d). Considering the fact that increased E_a(SEI) over time was observed for both Li-glyme and Na-glyme systems, the observed morphology and thickness of SEIs imply the densification (or compaction) of the SEIs. Note that the creep due to the pressure buildup in the cell causes the smoother surface of Na upon longer open-circuit potential storage.[39−41]

Similarly as glymes, carbonate-based electrolytes were in contact with Li/Na under open-circuit potential. The extracted E_a(SEI) before and after long open-circuit storage, corresponding cross-section images, and surface analyses of Li with XPS are available in the Supporting Information (details can be found in Supporting Information Figures S5, S6, S8-3, and S8-4). Densification of the SEI is observed for Li-carbonate and Na-carbonate systems (supported by the increase of E_a(SEI) in Figure S5) as well, and a porous SEI in the case of Na is evident from FIB-SEM (see Figure S6). For both glyme-based electrolyte and carbonate-based electrolyte cases, E_a(SEI) on Na is lower than E_a(SEI) of Li even after storage under open-circuit conditions for 600 h, implying that the SEI on Na is more porous than the SEI on Li. This claim is additionally supported by ToF-SIMS analyses of SEIs on Li/Na in the Supporting Information (Figure S7), where a clear distinction in roughness between Li and Na electrodes is shown. If the SEI is porous, electrolyte will permeate into the pores and upon electrode drying needed for sample preparation, only the solvent will evaporate, leaving the salt precipitated in the pores. Therefore, existence of the salt in the depth of the SEI is a clear indication of a porous SEI. For both Li-glyme and Li-carbonate systems (see Figure S7a,b), measured intensity of the salt anion ($CF_3SO_3^-$) decreases approximately three orders of magnitude (~0.001%, normalized intensity) after 600 s of sputtering. On the contrary, Na systems exhibit a significant amount of salt anion intensity (>0.1%) over 600 s of sputtering, implying the existence of salt in the bulk of the SEIs (see Figure S7c,d) and the porosity of SEIs. Note that here the sputtering time is not proportional to the sample depth and intensity is not directly proportional to the concentration of $CF_3SO_3^-$, since both parameters are dependent on the surface roughness, element type, and the matrix surrounding the element.

In the summary of the results of electrochemical (EIS), chemical (XPS and ToF-SIMS) and morphological (FIB-SEM) characterizations in four different Li/Na systems (Li-glyme, Li-carbonate, Na-glyme, and Na-carbonate), it is concluded that (i) SEIs become denser over time in both Li/Na systems and (ii) SEIs on Na are more porous compared to the SEIs on Li, leading to the continuous SEI growth, which is not over even after long-term aging. However, in the case when E_a > 0.5 is observed, we cannot exclude the possibility that the activation energy is affected by space charge layer formation between different SEI phases, suggested in recent theoretical studies.[42] For the special case of the initially formed (after 2 h) SEI on Na upon contact with glyme-based electrolytes, the E_a = 0.15 clearly indicates a porous SEI with predominant liquid pathways. Such low values of E_a are not possible for space charge zones as they always also contain additional migration contribution. We ascribe the higher porosity of SEIs on Na to the fact that the Pilling−Bedworth ratio of the expected inorganic Na SEI compounds is always lower than 1 (Table S2). On the other hand, several Li inorganic SEI compounds have an R_{PB} higher than 1, such as Li_2CO_3 (1.35), LiOH (1.26), and Li_2S (1.06), enabling SEIs of higher density. However, this picture is simplified and R_{PB} of organic SEI compounds should not be overlooked, once their exact molecular structure and composition are known.

3.3. Determination of the Salt Diffusion Coefficients and Cationic Transference Number of Salt-in-Solvent Electrolytes. Bulk properties of the liquid SEI such as $t_{Li(Na)}$ and D_{salt} were determined by the galvanostatic polarization method and the summary of results is shown in Table 1. Not only the transport behavior of SEIs but also the transport properties of electrolytes are of importance during stripping−plating, since they are directly correlated with Sand's time (i.e., characteristic time when salt concentration at the surface decreases to zero causing the dendrite to start growing).[43] Compared to Li, the transference number of Na is considerably higher in triglyme, which could be correlated either with the size of the ion and its higher mobility (consequence of the fact that Na is less solvated[44]) or to the specific molecular structure favoring positively charged ion aggregates containing Na. t_{Na} of carbonate-based electrolyte was difficult to be determined due to the high SEI resistance, making R_{SEI} and diffusion contribution not distinguishable (details can be found in Supporting Information part IX and Figure S9).

Table 1. Summary of the Cation Transference Numbers and Salt Diffusion Coefficients Derived from the Galvanostatic Polarization Method (Supporting Information, Figure S9)[a]

electrolytes	t_{pol}	D_{salt} ($cm^2\ s^{-1}$)
1M LiTf in triglyme	0.24	1.0×10^{-7}
1M LiTf in EC/DMC	0.12	2.8×10^{-6}
1M NaTf in triglyme	0.42 (t_{EIS} = 0.36)	1.7×10^{-6}
1M NaTf in EC/DMC	N/A	5.8×10^{-8}

[a] t_{EIS}: the transference number measured by the low-frequency EIS method (Supporting Information, Figure S10).

3.4. Stripping−Plating Behavior after Open-Circuit Aging of Li/Na Cells. The cyclic stripping−plating behavior was measured after aging under open-circuit potential directly after the cell assembly vs after 600 h of storage to investigate the overall performance of electrodes with SEIs formed in four different systems (Li-glyme, Na-glyme, Li-carbonate, and Na-carbonate). Figure 4 shows stripping−plating results of four symmetric cells where 0.1 mA cm^{-2} of constant current was applied for charging−discharging for 1 h each. In every case, stripping−plating behavior directly upon cell assembly (Figure 4, black) shows a more stable cycling behavior and lower overpotential compared to the cells stored for a long time (Figure 4, red). Indeed, the denser SEIs are beneficial for preventing further electrolyte decomposition but make the ion transport less facile as proven by the increased E_a, resulting in larger overpotential and cell failure. Comparing Li and Na behavior in an overall manner, Na exhibits more frequent intermittent overpotential spikes whereas Li shows a gradual

https://doi.org/10.1021/acsami.1c15607
ACS Appl. Mater. Interfaces 2021, 13, 51767−51774

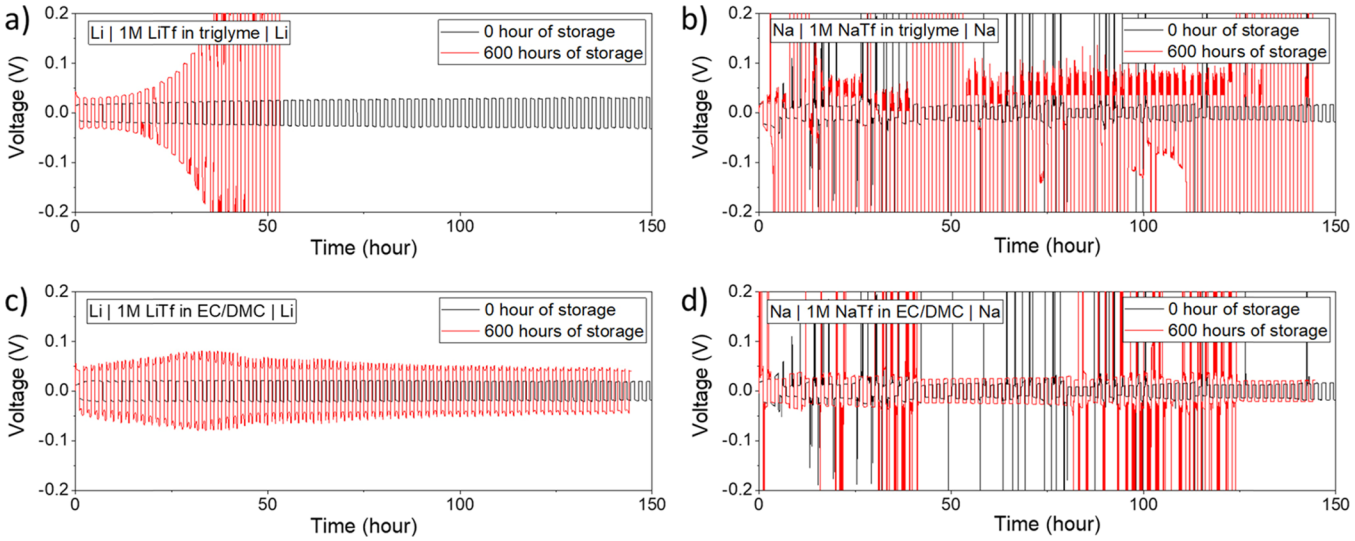

Figure 4. Stripping–plating behavior of symmetric Li/Na cells after initial cell assembly vs after 600 h of storage (applied current: 0.1 mA cm^{-2}) with (a,b) triglyme and (c,d) carbonate electrolytes. Top-view images of the electrode after stripping–plating measured by SEM are shown in Figure S11.

change of overpotential during cycling. This may be attributable to (i) chemically/mechanically unstable SEIs on Na[25−27] and (ii) relatively low values of D_{salt} of the Na-salt-containing electrolyte, shortening Sand's time.[45] However, many other factors affecting cycling behavior such as chemical/morphological homogeneity and mechanical properties of the SEIs should also be considered, which could be examined systematically with atomic force microscopy as it is recently shown in the literature.[46−49] Furthermore, it may not be neglected that stripping causes additional porosity or isolated metallic Li,[50,51] leading to altered Li^+/Na^+ transport properties during galvanostatic cycling. The top-view SEM images of the surface of the corresponding electrodes after stripping–plating are available in the Supporting Information (see Figure S11). No direct correlation between cycling behavior and morphology is observed.

4. CONCLUSIONS

We investigated the long-term (~a month) growth of SEIs on Li/Na metal electrodes with various nonaqueous liquid electrolytes under open-circuit potential and examined their ionic transport behavior over time. Glyme- and carbonate-based electrolytes were tested and compared in symmetric Li/Na cells. In every tested cell, SEIs densify over time (volume % increase of the solid phase on the account of the liquid phase) as confirmed by the increase of activation energy of the ionic transport (E_a). We propose this type of evaluation as a standard method to estimate the porosity of the SEI. Compared to Li, Na is found to form more porous SEIs as confirmed by lower E_a and the presence of salt anions in the bulk measured by ToF-SIMS. The porous SEI appears to have low SEI resistance at the initial stage of storage but leads to the continuous growth of the interface through densification process. Therefore, the porosity of the SEI should be carefully taken into account for the SEIs formed in contact with liquid/solid electrolytes, especially for the case of Na where porosity is unavoidable by the nature of the inorganic phases in the formed film ($R_{PB} < 1$). Likewise, it is highly recommended to focus on the thorough experimental investigation and control of porosity of artificially prepared SEIs on alkali metal electrodes. We do not exclude the possibility that the differences in the native film formation between Li and Na strongly affect the differences in the formed SEI, but examining it will require experimentally challenging and persistent efforts. Additionally, we observe for the first time a considerably higher salt diffusion coefficient and cation transference number in Na-glyme electrolytes compared to their lithium counterparts.

■ ASSOCIATED CONTENT

Supporting Information

The Supporting Information is available free of charge at https://pubs.acs.org/doi/10.1021/acsami.1c15607.

EIS results of symmetric Li/Na cells and symmetric stainless-steel cells with pure glyme solvents; ICP-OES results of pure triglyme solvent in contact with Li/Na; EIS results of Li/Na symmetric cells with pure carbonate solvent; E_a of ion transport in bulk electrolytes; time-dependent E_a of Li-carbonate and Na-carbonate systems; FIB-SEM images of SEIs on Li and Na in contact with carbonate-based electrolyte for 2 and 600 h; ToF-SIMS spectra of SEIs on Li and Na in contact with glyme-/carbonate-based electrolytes after 600 h of storage under open-circuit conditions; XPS spectra of SEIs on Li in contact with glyme-/carbonate-based electrolytes; determination of the cation transference number ($t_{Li/Na}$) and salt diffusion coefficient (D_{salt}) by the galvanostatic polarization method; t_{Na} determination by the Sørensen and Jacobsen method; top-view SEM images of Li/Na electrodes after stripping/plating with glyme-/carbonate-based electrolyte stored for 0 vs 600 h; comparison of the Pilling–Bedworth ratio (R_{PB}) of inorganic Li SEI compounds vs Na SEI compounds (PDF)

■ AUTHOR INFORMATION

Corresponding Author

Jelena Popovic − *Max Planck Institute for Solid State Research, Stuttgart 70569, Germany;* orcid.org/0000-0001-6618-4306; Email: popovic@fkf.mpg.de

Authors

Kyungmi Lim − *Max Planck Institute for Solid State Research, Stuttgart 70569, Germany*

Bernhard Fenk − *Max Planck Institute for Solid State Research, Stuttgart 70569, Germany*

Joachim Maier − *Max Planck Institute for Solid State Research, Stuttgart 70569, Germany;* orcid.org/0000-0003-2274-6068

Complete contact information is available at: https://pubs.acs.org/10.1021/acsami.1c15607

Funding

Open access funded by Max Planck Society.

Notes

The authors declare no competing financial interest.

■ ACKNOWLEDGMENTS

The authors thank Jürgen Weis for enabling FIB-SEM analyses, Kathrin Küster for the XPS measurements, Tolga Acartürk for ToF-SIMS investigation, and Samir Hammoud for ICP-OES. Florian Kaiser, Uwe Traub, and Udo Klock are acknowledged for their general technical support. Filip Podjaski is thanked for giving comments on the written manuscript.

■ REFERENCES

(1) Xu, W.; Wang, J.; Ding, F.; Chen, X.; Nasybulin, E.; Zhang, Y.; Zhang, J.-G. Lithium metal anodes for rechargeable batteries. *Energy Environ. Sci.* **2014**, *7*, 513−537.

(2) Lee, B.; Paek, E.; Mitlin, D.; Lee, S. W. Sodium Metal Anodes: Emerging Solutions to Dendrite Growth. *Chem. Rev.* **2019**, *119*, 5416−5460.

(3) Lin, D.; Liu, Y.; Cui, Y. Reviving the lithium metal anode for high-energy batteries. *Nat. Nanotechnol.* **2017**, *12*, 194−206.

(4) Zhang, Y.; Zuo, T.-T.; Popovic, J.; Lim, K.; Yin, Y.-X.; Maier, J.; Guo, Y.-G. Towards better Li metal anodes: Challenges and strategies. *Mater. Today* **2020**, *33*, 56−74.

(5) Peled, E. The electrochemical behavior of alkali and alkaline earth metals in nonaqueous battery systems—the solid electrolyte interphase model. 1979, *126* (12), 2047, DOI: 10.1149/1.2128859.

(6) Thevenin, J. G.; Muller, R. H. Impedance of Lithium Electrodes in a Propylene Carbonate Electrolyte. *J. Electrochem. Soc.* **1987**, *134*, 273−280.

(7) Zaban, A.; Zinigrad, E.; Aurbach, D. Impedance Spectroscopy of Li Electrodes. 4. A General Simple Model of the Li−Solution Interphase in Polar Aprotic Systems. *J. Phys. Chem.* **1996**, *100*, 3089−3101.

(8) Montesperelli, G.; Nunziante, P.; Pasquali, M.; Pistoia, G. Li passivation in different electrolytes during storage and cycling — An impedance spectroscopy study. *Solid State Ionics* **1990**, *37*, 149−156.

(9) Aurbach, D.; Zaban, A. Impedance spectroscopy of lithium electrodes: Part 1. General behavior in propylene carbonate solutions and the correlation to surface chemistry and cycling efficiency. *J. Electroanal. Chem.* **1993**, *348*, 155−179.

(10) Geronov, Y.; Schwager, F.; Muller, R. Film formation on lithium in propylene carbonate solutions under open circuit Conditions. 1980, *129* (LBL-11126), 91687731, DOI: 10.1149/1.2124177.

(11) Kanamura, K.; Tamura, H.; Shiraishi, S.; Takehara, Z.-I. Morphology and chemical compositions of surface films of lithium deposited on a Ni substrate in nonaqueous electrolytes. *J. Electroanal. Chem.* **1995**, *394*, 49−62.

(12) Shiraishi, S.; Kanamura, K.; Takehara, Z.-I. Study of the Surface Composition of Highly Smooth Lithium Deposited in Various Carbonate Electrolytes Containing HF. *Langmuir* **1997**, *13*, 3542−3549.

(13) Aurbach, D.; Markovsky, B.; Levi, M. D.; Levi, E.; Schechter, A.; Moshkovich, M.; Cohen, Y. New insights into the interactions between electrode materials and electrolyte solutions for advanced nonaqueous batteries. *J. Power Sources* **1999**, *81*−*82*, 95−111.

(14) Odziemkowski, M.; Irish, D. E. An Electrochemical Study of the Reactivity at the Lithium Electrolyte/Bare Lithium Metal Interface: II. Unpurified Solvents. *J. Electrochem. Soc.* **1993**, *140*, 1546−1555.

(15) Peled, E.; Golodnitsky, D.; Ardel, G. Advanced Model for Solid Electrolyte Interphase Electrodes in Liquid and Polymer Electrolytes. *J. Electrochem. Soc.* **1997**, *144*, L208−L210.

(16) Wang, A.; Kadam, S.; Li, H.; Shi, S.; Qi, Y. Review on modeling of the anode solid electrolyte interphase (SEI) for lithium-ion batteries. *npj Comput. Mater.* **2018**, *4*, 15.

(17) Liu, D.; Shadike, Z.; Lin, R.; Qian, K.; Li, H.; Li, K.; Wang, S.; Yu, Q.; Liu, M.; Ganapathy, S.; Qin, X.; Yang, Q.-H.; Wagemaker, M.; Kang, F.; Yang, X.-Q.; Li, B. Review of Recent Development of In Situ/Operando Characterization Techniques for Lithium Battery Research. 2019, *31* (28), 1806620, DOI: 10.1002/adma.201806620.

(18) Tripathi, A. M.; Su, W.-N.; Hwang, B. J. In situ analytical techniques for battery interface analysis. *Chem. Soc. Rev.* **2018**, *47*, 736−851.

(19) Lin, F.; Liu, Y.; Yu, X.; Cheng, L.; Singer, A.; Shpyrko, O. G.; Xin, H. L.; Tamura, N.; Tian, C.; Weng, T.-C.; Yang, X.-Q.; Meng, Y. S.; Nordlund, D.; Yang, W.; Doeff, M. M. Synchrotron X-ray Analytical Techniques for Studying Materials Electrochemistry in Rechargeable Batteries. *Chem. Rev.* **2017**, *117*, 13123−13186.

(20) Tan, D. H. S.; Banerjee, A.; Chen, Z.; Meng, Y. S. From nanoscale interface characterization tosustainable energy storage using all-solid-statebatteries. *Nat. Nanotechnol.* **2020**, *15*, 170−180.

(21) Zhou, Y.; Su, M.; Yu, X.; Zhang, Y.; Wang, J.-G.; Ren, X.; Cao, R.; Xu, W.; Baer, D. R.; Du, Y.; Borodin, O.; Wang, Y.; Wang, X.-L.; Xu, K.; Xu, Z.; Wang, C.; Zhu, Z. Real-time mass spectrometric characterization of the solid−electrolyte interphase of a lithium-ion battery. *Nat. Nanotechnol.* **2020**, *15*, 224−230.

(22) Han, B.; Zou, Y.; Zhang, Z.; Yang, X.; Shi, X.; Meng, H.; Wang, H.; Xu, K.; Deng, Y.; Gu, M. Probing the Na metal solid electrolyte interphase via cryo-transmission electron microscopy. *Nat. Commun.* **2021**, *12*, 3066.

(23) Boyle, D. T.; Huang, W.; Wang, H.; Li, Y.; Chen, H.; Yu, Z.; Zhang, W.; Bao, Z.; Cui, Y. Corrosion of lithium metal anodes during calendar ageing and its microscopic origins. *Nat. Energy* **2021**, 487.

(24) Wood, S. M.; Fang, C.; Dufek, E. J.; Nagpure, S. C.; Sazhin, S. V.; Liaw, B.; Meng, Y. S. Predicting Calendar Aging in Lithium Metal Secondary Batteries: The Impacts of Solid Electrolyte Interphase Composition and Stability. 2018, *8* (26), 1801427, DOI: 10.1002/aenm.201801427.

(25) Iermakova, D. I.; Dugas, R.; Palacín, M. R.; Ponrouch, A. On the Comparative Stability of Li and Na Metal Anode Interfaces in Conventional Alkyl Carbonate Electrolytes. *J. Electrochem. Soc.* **2015**, *162*, A7060−A7066.

(26) Mandl, M.; Becherer, J.; Kramer, D.; Mönig, R.; Diemant, T.; Behm, R. J.; Hahn, M.; Böse, O.; Danzer, M. A. Sodium metal anodes: Deposition and dissolution behaviour and SEI formation. *Electrochim. Acta* **2020**, *354*, No. 136698.

(27) Mogensen, R.; Brandell, D.; Younesi, R. Solubility of the Solid Electrolyte Interphase (SEI) in Sodium Ion Batteries. *ACS Energy Lett.* **2016**, *1*, 1173−1178.

(28) Nojabaee, M.; Popovic, J.; Maier, J. Glyme-based liquid−solid electrolytes for lithium metal batteries. *J. Mater. Chem. A* **2019**, *7*, 13331−13338.

(29) Otto, S.-K.; Moryson, Y.; Krauskopf, T.; Peppler, K.; Sann, J.; Janek, J.; Henss, A. In-Depth Characterization of Lithium-Metal Surfaces with XPS and ToF-SIMS: Toward Better Understanding of the Passivation Layer. *Chem. Mater.* **2021**, *33*, 859−867.

(30) Kamphaus, E. P.; Angarita-Gomez, S.; Qin, X.; Shao, M.; Engelhard, M.; Mueller, K. T.; Murugesan, V.; Balbuena, P. B. Role of Inorganic Surface Layer on Solid Electrolyte Interphase Evolution at Li-Metal Anodes. *ACS Appl. Mater. Interfaces* **2019**, *11*, 31467−31476.

(31) Peled, E.; Menkin, S. Review—SEI: Past, Present and Future. *J. Electrochem. Soc.* **2017**, *164*, A1703−A1719.
(32) Shi, S.; Lu, P.; Liu, Z.; Qi, Y.; Hector, L. G.; Li, H.; Harris, S. J. Direct Calculation of Li-Ion Transport in the Solid Electrolyte Interphase. *J. Am. Chem. Soc.* **2012**, *134*, 15476−15487.
(33) Peled, E.; Golodnitsky, D.; Ardel, G.; Eshkenazy, V. The sei model—application to lithium-polymer electrolyte batteries. *Electrochim. Acta* **1995**, *40*, 2197−2204.
(34) Berhaut, C. L.; Lemordant, D.; Porion, P.; Timperman, L.; Schmidt, G.; Anouti, M. Ionic association analysis of LiTDI, LiFSI and LiPF6 in EC/DMC for better Li-ion battery performances. *RSC Adv.* **2019**, *9*, 4599−4608.
(35) Pfaffenhuber, C.; Hoffmann, F.; Fröba, M.; Popovic, J.; Maier, J. Soggy-sand effects in liquid composite electrolytes with mesoporous materials as fillers. *J. Mater. Chem. A* **2013**, *1*, 12560−12567.
(36) Lorger, S.; Usiskin, R.; Maier, J. Transport and Charge Carrier Chemistry in Lithium Oxide. *J. Electrochem. Soc.* **2019**, *166*, A2215−A2220.
(37) Mizusaki, J.; Tagawa, H.; Saito, K.; Uchida, K.; Tezuka, M. Lithium carbonate as a solid electrolyte. *Solid State Ionics* **1992**, *53*−*56*, 791−797.
(38) Lorger, S.; Usiskin, R. E.; Maier, J. Transport and Charge Carrier Chemistry in Lithium Sulfide. 2019, *29* (6), 1807688, DOI: 10.1002/adfm.201807688.
(39) Fincher, C. D.; Zhang, Y.; Pharr, G. M.; Pharr, M. Elastic and Plastic Characteristics of Sodium Metal. *ACS Appl. Energy Mater.* **2020**, *3*, 1759−1767.
(40) Wang, M. J.; Chang, J.-Y.; Wolfenstine, J. B.; Sakamoto, J. Analysis of elastic, plastic, and creep properties of sodium metal and implications for solid-state batteries. *Materialia* **2020**, *12*, No. 100792.
(41) Zhang, X.; Wang, Q. J.; Peng, B.; Wu, Y. Pressure-Driven and Creep-Enabled Interface Evolution in Sodium Metal Batteries. *ACS Appl. Mater. Interfaces* **2021**, 26533.
(42) Zhang, Q.; Pan, J.; Lu, P.; Liu, Z.; Verbrugge, M. W.; Sheldon, B. W.; Cheng, Y.-T.; Qi, Y.; Xiao, X. Synergetic Effects of Inorganic Components in Solid Electrolyte Interphase on High Cycle Efficiency of Lithium Ion Batteries. *Nano Lett.* **2016**, *16*, 2011−2016.
(43) Bai, P.; Li, J.; Brushett, F. R.; Bazant, M. Z. Transition of lithium growth mechanisms in liquid electrolytes. *Energy Environ. Sci.* **2016**, *9*, 3221−3229.
(44) Usiskin, R.; Lu, Y.; Popovic, J.; Law, M.; Balaya, P.; Hu, Y.-S.; Maier, J. Fundamentals, status and promise of sodium-based batteries. *Nat. Rev. Mater.* **2021**, DOI: 10.1038/s41578-021-00324-w.
(45) Brissot, C.; Rosso, M.; Chazalviel, J. N.; Lascaud, S. Dendritic growth mechanisms in lithium/polymer cells. *J. Power Sources* **1999**, *81*−*82*, 925−929.
(46) Yoon, I.; Jurng, S.; Abraham, D. P.; Lucht, B. L.; Guduru, P. R. Measurement of mechanical and fracture properties of solid electrolyte interphase on lithium metal anodes in lithium ion batteries. *Energy Storage Mater.* **2020**, *25*, 296−304.
(47) Liu, Q.; Zhang, L.; Sun, H.; Geng, L.; Li, Y.; Tang, Y.; Jia, P.; Wang, Z.; Dai, Q.; Shen, T.; Tang, Y.; Zhu, T.; Huang, J. In Situ Observation of Sodium Dendrite Growth and Concurrent Mechanical Property Measurements Using an Environmental Transmission Electron Microscopy−Atomic Force Microscopy (ETEM-AFM) Platform. *ACS Energy Lett.* **2020**, *5*, 2546−2559.
(48) Cohen, Y. S.; Cohen, Y.; Aurbach, D. Micromorphological Studies of Lithium Electrodes in Alkyl Carbonate Solutions Using in Situ Atomic Force Microscopy. *J. Phys. Chem. B* **2000**, *104*, 12282−12291.
(49) Mogi, R.; Inaba, M.; Abe, T.; Ogumi, Z. In situ atomic force microscopy observation of lithium deposition at an elevated temperature. *J. Power Sources* **2001**, *97*−*98*, 265−268.
(50) Fang, C.; Li, J.; Zhang, M.; Zhang, Y.; Yang, F.; Lee, J. Z.; Lee, M.-H.; Alvarado, J.; Schroeder, M. A.; Yang, Y.; Lu, B.; Williams, N.; Ceja, M.; Yang, L.; Cai, M.; Gu, J.; Xu, K.; Wang, X.; Meng, Y. S. Quantifying inactive lithium in lithium metal batteries. *Nature* **2019**, *572*, 511−515.
(51) Cho, J. H.; Xiao, X.; Guo, K.; Liu, Y.; Gao, H.; Sheldon, B. W. Stress evolution in lithium metal electrodes. *Energy Storage Mater.* **2020**, *24*, 281−290.